PREDICTING FIBRE KINKING AND SPLITTING USING A FINITE FRACTURE MECHANICS FORMULATION

R. Gutkin[1*], S.T. Pinho[2]

[1]*Swerea Sicomp AB, Box 104, SE-431 22 Mölndal, Sweden*
[2]*Department of Aeronautics, Imperial College London, UK*
renaud.gutkin@swerea.se

Keywords: Fracture mechanics, kink-band, splitting, failure criterion

Abstract
This paper presents the development of a model to predict the strength associated with kink-band formation and fibre splitting based on a finite fracture mechanics approach. The model is derived to handle tri-axial stress states, namely longitudinal compression combined with in-plane shear and hydrostatic pressure. Correlations with experimental data from the literature show that the physics of the problem is correctly captured.

1. Introduction
Longitudinal compressive failure of composites has been a very active field of research for many decades because of the complexity of the failure modes triggered, the difficulty of obtaining detailed and reliable experimental evidences and the high sensitivity of the compressive strength to defects and multi-axial stress states. Experimental investigations have shown that three failure modes are to be expected in longitudinal compression, namely: fibre kinking, fibre splitting and shear-driven fibre compressive failure, as shown in Figure 1a, b and c, respectively.

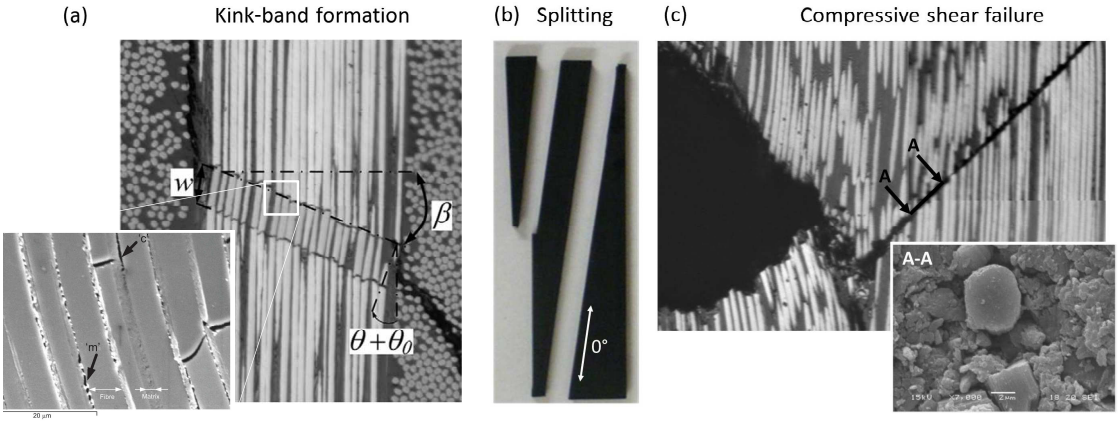

Figure 1. Failure modes in longitudinal compression.

The present contribution focuses on fibre kinking and fibre splitting which are often considered as the most common failure modes. Fibre kinking typically initiates in areas of misaligned fibres. These fibres rotate under a compressive load, and the shear stresses induced in the matrix lead to matrix failure and kink-band formation. In the closeup view

Figure 1a, microcracks in the resin are observed, labelled 'm'. Some of these microcracks have coalesced to form a split, labelled 'c'.
Fibre splitting is also controlled by matrix failure but is more often found under large shear stresses combined with longitudinal compression. On the contrary to kink-band formation, fibre splitting failures do not localize and can extend over large part of a component as shown in Figure 1b.
Many models, both analytical and numerical, have been developed to predict the strength associated with kink-band formation. Models capturing best experimental trends commonly assume the sequence of events described above and are referred as kinking theory. These models typically neglect the bending contribution of the fibres and represent the kink-band as a band of material with orthotropic material properties rotated in the misaligned coordinate system of the fibres (angle $\theta+\theta_0$). The longitudinal compressive strength is then evaluated when yielding of the matrix in the band is reached.
More recently, Dàvila and Camanho in [1] proposed a criterion for fibre kinking, whereby the stress applied on a unidirectional composite, containing a region of misaligned fibres, is rotated in that misaligned coordinate system. The resolved stresses are then used to evaluate the LaRC matrix failure criterion to test for failure. This approach was developed further in [2] to account for the nonlinear response of the composite in shear as well as to handle 3D loading situations.
In this contribution, the formulation of an analytical model developed in [3] for combined in-plane shear and longitudinal compression is summarised and an extension to handle hydrostatic stress state is presented. The model is based on a fracture mechanics approach which offers a better representation of microcracking in brittle resins and contrasts to previous models [4-7] based on a plasticity approach and more appropriate to ductile resins. Finally, the results of the model are compared to experimental data available in the literature and discussed.

2. Model formulation

2.1. Framework

The model and criterion derived here are applicable for failure by kink-band formation and fibre splitting for relatively high fibre volume fraction, typical of high performance composites, where longitudinal compressive failure is by fibre kinking/splitting. The experimental observations show that kink-band initiation results from the formation of matrix microcracks and splits in the inter-fibre region. Therefore, the present model is based on the hypothesis that the strength associated with fibre kinking is reached when the strain energy released, per unit area of crack generated between an undamaged state and a damaged state, is equal to the energy required to create a unit area of cracks (fracture energy).
To calculate the strain and fracture energies, some simplifications and assumptions on the geometry, loading conditions and material response are made and listed below.
More details on the derivations for the case of in-plane shear and longitudinal compression are given in [3].

Simplifications

S(i) The control volume (Figure 2a) chosen is a representative element of material in the kink-band. The model is 2D with fibres considered to be perfect cylinders of diameter ϕ_f and arranged in a hexagonal pattern with a fibre volume fraction v_f. The model has a unit thickness (in the 3-direction), and is taken from one of the symmetry planes of the fibre arrangement.
A fibre volume fraction for the 2D equivalent model can also be defined as

$$v_f^{2D} = \frac{\phi_f}{\phi_f + t_m} \qquad \text{Equation 1}$$

where t_m is the thickness of the matrix layer.

S(ii) Fibre bending is neglected and the fibres are considered to be incompressible.

S(iii) The deformation of the matrix due to the rotation of the kink-band to the propagation angle β is neglected.

S(iv) The matrix transmits only shear stresses. The shear stresses are considered uniform across the matrix layer. The fibres are assumed parallel to each other, and to remain so during loading, as the matrix deforms predominantly in shear.

Assumptions

A(i) When a nonlinear shear response of the matrix is considered, the nonlinearities are assumed to be induced by damage alone.

A(ii) Crack formation between the undamaged state (A) and damage state (B), Figure 2a, is assumed to occur at constant displacement and the kinetic energy is neglected.

A(iii) The microcracks have complex shapes and distribution, and their actual area is not observable. Hence, it is assumed that the area of the microcracks created per unit of thickness, for a width *w* of kink-band, can be written as

$$\alpha w t_m \qquad \text{Equation 2}$$

where the coefficient α is an undetermined proportionality factor and has for dimension $[\text{mm}]^{-1}$

A(iv) Matrix cracking is assumed to occur under a certain mixed mode critical energy release rate G_c.

A(v) The hydrostatic pressure is assumed to not affect the equilibrium of the fibre and to only contribute to the strain energy.

A(vi) The product $\alpha.G_c$ and the resin Young's and shear moduli, E_m and G_m, are function of the hydrostatic pressure.

2.2. Equilibrium of the fibre

The strain energy stored in the control volume is obtained from the equilibrium of a fibre of length *w*, initially misaligned at an angle θ_0, and subjected to an axial force P, a shear force S (the forces P and S are per unit width, see *S*(i)) and an hydrostatic pressure σ_p, see Figure 2b. Under the action of the axial and shear forces–the hydrostatic pressure is in equilibrium on the fibre *A*(v)– the fibre rotates by an additional angle θ, such that at equilibrium, the fibre is at an angle $\theta_0 + \theta$.

$$P\theta + P\theta_0 - \tau_m \phi_f w + Sw = 0 \qquad \text{Equation 3}$$

The axial and shear forces acting on the fibre can be expressed in terms of the homogenised applied stresses

$$\sigma_{11} \sim \frac{P}{\phi_f} v_f^{2D} \qquad \text{Equation 4;} \qquad \tau_{12} \sim \frac{S}{\phi_f} \qquad \text{Equation 5}$$

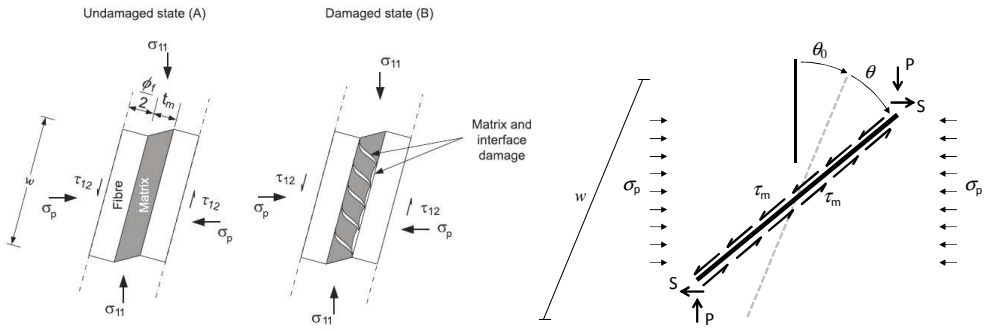

Figure 2. (a) Assumed formation of microcracks during kink-band formation; (b) Equilibrium of the fibre.

So that the equilibrium of the fibre finally reads

$$\sigma_{11}\frac{(\theta+\theta_0)}{v_f^{2D}}+\tau_{12}=f_{CL}^{\theta}(\theta) \qquad \text{Equation 6}$$

with the shear stress in the matrix $\tau_m = f_{CL}^{\theta}(\theta)$, and f_{CL}^{θ} is a generic function relating the shear stress and the shear strain.

2.3. Strain energy and dissipated fracture energy

Using the simplifications *S*(ii) and *S*(iv), the strain energy of the model in the undamaged state A, see Figure 2a, reduces to the strain energy stored in the matrix

$$U_A = U_m = \frac{1}{2}\int_{V_m}\tau_m\gamma_m dV + \frac{1}{2}\int_{V_m}\sigma_p\varepsilon_p^m dV \qquad \text{Equation 7}$$

which can be rewritten as

$$U_A = \frac{1}{2}t_m w\left[\frac{\theta}{1-v_f^{2D}}f_{CL}^{\theta}(\theta)+\left(1-v_f^{2D}\right)\frac{{\sigma_p}^2}{E_m}\right] \qquad \text{Equation 8}$$

In the damaged state B, the element is considered fully damaged (the matrix does not resist any stresses) and $U_B = 0$.

Under assumptions *A*(iii) and *A*(iv) and with Equation 2, the fracture energy dissipated from state A to state B is written as

$$\Delta G = \alpha w t_m G_c \qquad \text{Equation 9}$$

2.4. Energy balance

In a general case, and with assumption *A*(ii), the energy balance during crack formation reads

$$\Delta W - \Delta U = \Delta G \qquad \text{Equation 10}$$

where ΔW is the work of the external forces. At constant displacement, the work is zero and the energy balance becomes

$$U_A = \Delta G \qquad \text{Equation 11}$$

Or using equations 7 and 9

$$\left[\frac{\theta}{1-v_f^{2D}} f_{CL}^{\theta}(\theta) + \left(1-v_f^{2D}\right)\frac{{\sigma_p}^2}{E_m}\right] = 2\alpha G_c \qquad \text{Equation 12}$$

2.5. Linear elastic shear response of the matrix
In the case of a linear elastic matrix, with

$$\tau_m = f_{CL}^{\theta}(\theta) = G_m \frac{\theta}{\left(1-v_f^{2D}\right)} \qquad \text{Equation 13}$$

The angle of rotation of the fibres is related to the applied stresses by using Equation 6 so that

$$\theta = \frac{\tau_{12} v_f^{2D} + \sigma_{11}\theta_0}{\frac{G_m}{\left(1-v_f^{2D}\right)} v_f^{2D} - \sigma_{11}} \qquad \text{Equation 14}$$

Which, replaced in Equation 12, and after simplifications, gives

$${\tau_{12}}^2 + \frac{2\sigma_{11}\theta_0}{v_f^{2D}}\tau_{12} + \left[\left(\frac{\sigma_{11}\theta_0}{v_f^{2D}}\right)^2 - \frac{1}{G_m}\left(G_m - \frac{1-v_f^{2D}}{v_f^{2D}}\sigma_{11}\right)^2\left(2\alpha G_c - \frac{{\sigma_p}^2}{E_m}\right)\right] = 0 \qquad \text{Equation 15}$$

3. Discussion on some particular forms of the model

3.1. Combined in-plane shear and hydrostatic pressure
For $\sigma_{11} = 0$ and $\sigma_p \neq 0$, Equation 15 becomes

$${\tau_{12}}^2 + G_m\left(2\alpha G_c - \frac{{\sigma_p}^2}{E_m}\right) = 0 \qquad \text{Equation 16}$$

The solution of this equation gives the shear stress at failure, in-plane shear strength S_L, as a function of the hydrostatic pressure, but note that α.G_c, E_m and G_m are also function of σ_p

$$\tau_{12} = S_L(\sigma_p) = \pm\sqrt{G_m\left(2\alpha G_c - \frac{{\sigma_p}^2}{E_m}\right)} \qquad \text{Equation 17}$$

3.2. Combined longitudinal compression and hydrostatic pressure
Taking $\tau_{12} = 0$ in Equation 15, we obtain

$$\left[\left(\frac{\sigma_{11}\theta_0}{v_f^{2D}}\right)^2 - \frac{1}{G_m}\left(G_m - \frac{1-v_f^{2D}}{v_f^{2D}}\sigma_{11}\right)^2\left(2\alpha G_c - \frac{{\sigma_p}^2}{E_m}\right)\right] = 0 \qquad \text{Equation 18}$$

Taking the square root and replacing $2\alpha G_c - \frac{{\sigma_p}^2}{E_m}$ by $S_L(\sigma_p)/G_m$, an expression of the longitudinal stress at failure, longitudinal strength, is found

$$X_C = \frac{v_f^{2D} S_L(\sigma_p)}{\frac{1 - v_f^{2D}}{G_m} S_L(\sigma_p) + \theta_0}$$ Equation 19

This equation is identical to Budiansky's formula [8] if we note that micromechanically $G_m/1 - v_f^{2D}$ corresponds to the in-plane shear modulus of the composite and therefore $1 - v_f^{2D}/G_m . S_L(\sigma_p)$ is the shear strain at failure. However, Equation 19 shows how the hydrostatic pressure affects the longitudinal compressive through the shear modulus and shear strength of the composites.

3.3. Combined in-plane shear and longitudinal compression

Finally, for $\sigma_p = 0$, Equation 15 has for solution (α.G_c, E_m and G_m, are denoted here with a subscript $_0$ to emphasize that their values is for $\sigma_p = 0$)

$$\tau_{12} = -\frac{\sigma_{11}\theta_0}{v_f^{2D}} + \frac{(1 - v_f^{2D})}{v_f^{2D}} \sqrt{2\left(\alpha G_c / G_m\right)_0 \left(\frac{(G_m)_0}{(1 - v_f^{2D})} v_f^{2D} - \sigma_{11}\right)}$$ Equation 20

which becomes

$$\frac{\tau_{12}}{\sqrt{2(\alpha G_c G_m)_0}} + \frac{\sigma_{11}}{v_f^{2D}} \left(\frac{(1 - v_f^{2D})}{(G_m)_0} + \frac{\theta_0}{\sqrt{2(\alpha G_c G_m)_0}}\right) = 1$$ Equation 21

An expression for the in-plane shear strength is found as

$$S_L = \sqrt{2(\alpha G_c G_m)_0}$$ Equation 22

3.4. How do the micromechanical parameters related to ply properties?

It is interesting to look in detail at Equation 17 which relates strength properties at the microscale with those at the ply scale. When the hydrostatic pressure is zero, this equation reduces to Equation 22 which shares similarity to the equation derived in [9] for the in-situ shear strength of a thin ply embedded in a laminate.

$$S_L^{is} = \sqrt{8\, G_{IIc} G_{12}/\pi h}$$ Equation 23

The term α, with dimension mm^{-1}, is similar to the term 1/*h* in Equation 24, and accounts for two characteristics of the microcracks: (i) a crack density ρ, and (ii) a measure of their actual normalised area β, so that $\alpha = \rho\beta$. The term G_c in Equation 22 is in fact a mixed-mode toughness which would correspond to G_{IIC} in Equation 24 – even though G_c might be closer to G_{Ic} as shear cusps form in mode I.

In many respects, Equation 22 could be seen as an in-situ strength of the resin between fibres. The exact values of ρ, β and the mixed-mode ratio are of course difficult to measure practically but with Equation 22 they do not need to be known, as they are implicitly defined through the shear strength of the composite.

In Equation 17, it should be noted that the necessary condition $2\alpha G_c > {\sigma_p}^2/E_m$ is fulfilled in most cases as $2\alpha G_c$ and E_m will increase with increasing σ_p.

4. Prediction of failure envelopes

4.1. Shear and compression

Figure 3 shows a failure envelope for in-plane shear combined with longitudinal compression. The present model, Equation 21, is used with the material properties given in Table 1 and the model compared to experimental data from [4]. The model captures well the experimental trend and shows that increasing initial fibre misalignment results in lowered compressive strength.

θ_0 (˚)	S_L (MPa)	ϕ_f (mm)	v_f (%)	G_m (MPa)
2.1 and 2.5	75	7	60	1100

Table 1. Material properties used for Figure 3.

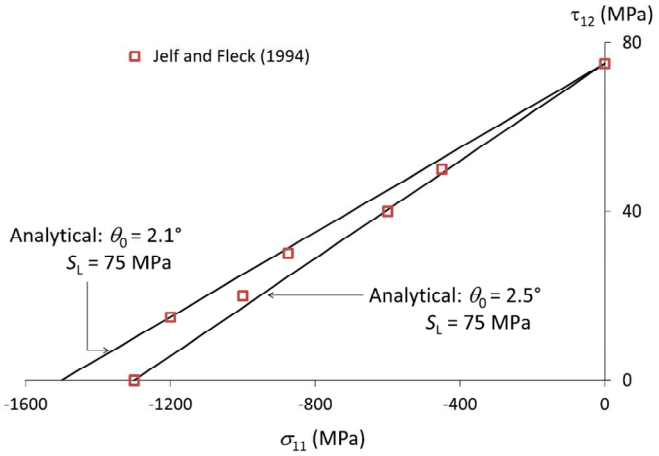

Figure 3. Failure envelope for in-plane shear combined with longitudinal compression [4].

4.2. Hydrostatic pressure and compression

Figure 4 shows a failure envelope for in-plane shear combined with longitudinal compression. The present model, Equation 19, is used with the material properties given in Table 2 and the model is compared to experimental data published in [11].

θ_0 (˚)	S_L (MPa)	ϕ_f (mm)	v_f (%)	G_m (MPa)
1.8	59	7	60	1320

Table 2. Material properties used for Figure 4.

Furthermore, because of the lack of data, G_m is assumed to be constant with the hydrostatic pressure and the shear strength to vary linearly with it

$$S_L = S_0 + \mu\sigma_p \qquad \text{Equation 24}$$

The coefficient μ is similar to the coefficient of friction used in [2,10]. For CFRP, it is recommended that $0.2<\mu<0.3$ [10] so it was chosen here to use μ = {0.25/0.3/0.35} as representative values.

The model predicts a nonlinear increase of the longitudinal compressive strength with increasing hydrostatic pressure, which reflects well experimental data. A good quantitative agreement is also achieved for the values of μ recommended in [10].

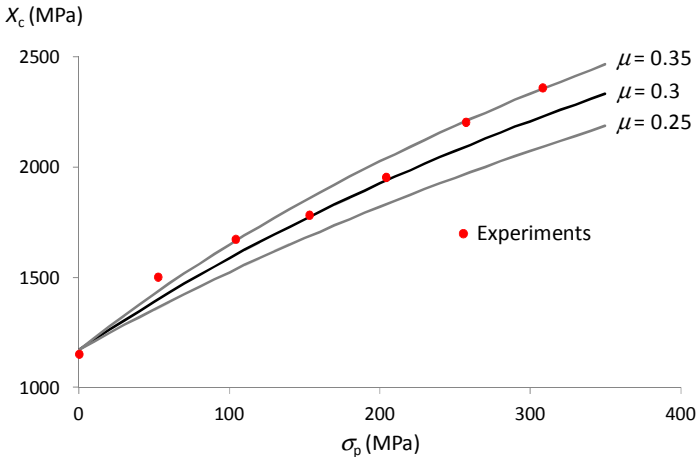

Figure 4. Longitudinal compressive strength versus hydrostatic pressure [11].

5. Conclusions

A model to predict the strength of fibre kinking and splitting under combined stress state and based on finite fracture mechanics has been presented. The model is able to capture experimental trends for longitudinal compression combined with in-plane shear and hydrostatic pressure.

References

[1] Dávila C.G., Camanho P.P. Failure criteria for FRP laminates in plane stress. *NASA Technical report TM-2003-212663*, (2003).

[2] Pinho S.T., Iannucci L., Robinson P. Physically-based failure models and criteria for laminated fibre-reinforced composites with emphasis on fibre kinking: Part I: Development. *Composites, PartA: Applied Science and Manufacturing*, **37**, pp. 63–73 (2006).

[3] Gutkin R., Pinho S.T., Robinson P., Curtis P.T. A finite fracture mechanics formulation to predict fibre kinking and splitting in CFRP under combined longitudinal compression and in-plane shear. *Mechanics of Materials*, **43**, pp. 730–739 (2011).

[4] Jelf P.M., Fleck N.A. The failure of composite tubes due to combined compression and torsion. *Journal of materials science*, **29**, pp. 3080–3084 (1994).

[5] Argon, A. Fracture of composites. *Treatise on Material Science and Technology*, **1**, pp. 79–114 (1972).

[6] Fleck N. Compressive failure of fiber composites. *Advances in applied mechanics*, **33**, pp. 43–117 (1997).

[7] Pimenta S., Gutkin R., Pinho S.T., Robinson P. A micromechanical model for kink-band formation: Part II—Analytical modelling. *Composites Science and Technology*, **69**, pp. 956–964 (2009).

[8] Budiansky, B., Fleck, N. Compressive failure of fibre composites. *Journal of mechanics and physics of solids*, **41**, pp. 183–211 (1993).

[9] Camanho P.P., Dàvila C.G., Pinho S.T., Iannucci L., Robinson P. Prediction of in situ strengths and matrix cracking in composites under transverse tension and in-plane shear. *Composites, Part A: Applied Science and Manufacturing*, **37**, pp. 165–176 (2006).

[10] Puck A., Kopp J., Knops M. Puck Guidelines for the determination of the parameters in Puck's action plane strength criterion. *Composites Science and Technology*, **62**, pp. 371–378 (2002).

[11] Wronsky AS, Parry TV. Compressive failure and kinking in uniaxially aligned glass-resin composite under superposed hydrostatic pressure. *Journal of Materials Science*, **17**, pp. 3656–62.